Joint European Research Infrastructure network for Coastal Observatory – Novel European eXpertise for coastal observaTories - **JERICO-NEXT**	
Deliverable title	Improved radar DA technology for biochemical transport analysis
Work Package Title	WP 3, Task 3.7
Deliverable number	D3.12
Description	Optimisation of 3D transport in the German Bight using additional information from tide gauges and ADCP data. Free model runs and analysis will be compared in terms of transports and langrangean trajectories. A radar observation model will be implemented in AIFS-DA EnKF in collaboration with CNR-ISMAR. This will be first evaluated in a quick OSSE assuming radar locations as for the actual radar observations in Gargano and in Gulf of Manfredonia (CNR-ISMAR) and then in OSEs for the same coastal region in WP4
Lead beneficiary	HZG
Lead Authors	Johannes Schulz-Stellenfleth, Eric Jansen
Contributors	CMCC, HZG, CNR-ISMAR
Submitted by	Stefania Ciliberti
Revision number	V1.1
Revision Date	12/10/2017
Security	Consortium Only or Public

History				
Revision	**Date**	**Modification**		**Author**
V1.1	12/10/17	Document in the right template, minor typos corrections		S. Ciliberti

Approvals				
	Name	**Organisation**	**Date**	**Visa**
Coordinator	Farcy Patrick	Ifremer		PF
WP Leaders	Petihakis George Delauney Laurent	HCMR Ifremer	16 October 2017	

PROPRIETARY RIGHTS STATEMENT

Table of contents

1   Executive Summary

The benefit of data assimilation techniques for the estimation of transports is discussed for two coastal areas in Europe with very different ocean circulation characteristics. The focus is on transport parameters, which are of concern for the transports of biological and chemical substances.

The first test case is located in the Western Adriatic Sea, in particular in the Gulf of Manfredonia, where a HF radar network has been successfully installed by CNR ISMAR. The first objective, here described, is to develop a novel HF radar operator to embed into a high resolution ocean model: the Adriatic-Ionian Forecasting System, developed at CMCC, has been used to In the present study, a novel HF radar operator for data assimilation has been developed for the Adriatic-Ionian Forecasting System – Ensemble Kalman Filter data assimilation system and used for assimilating radial velocity in the area of the Gulf of Manfredonia.

The German Bight is an example of a very shallow and tidal dominated coastal area, which is strongly affected by bottom friction processes and small scale bathymetry features. For this region a 4DVAR assimilation system was implemented based on a three dimensional barotropic circulation model and the respective adjoint model. A setup with 1 km spatial resolution and 5 sigma layers was considered for the analysis. On the observation side measurements from three HF radar stations as well as tide gauge data and ADCP data were used. The tide gauge measurements provide additional information on volume transports, which are not fully contained in the surface current estimates provided by the HF radar. The ADCP provides valuable information on the vertical current distribution. Different sources of model errors were considered in the analysis. The focus was on errors which affect the model performance in a systematic way, such as errors in bottom roughness, errors in the drag coefficients for wind forcing and internal friction parameters associated with turbulence. The respective parameters were optimised using the adjoint model combined with a conjugate gradient method. It turned out that the analysed model run shows good agreement with the HF radar data and excellent agreement with both the tide gauge and the ADCP. The analysed model run was used for different transport and drift calculations and compared with first guess runs, which were characterised by deviating parameter settings. Special focus was put on the role of the bottom friction and the momentum diffusion at the surface, which can for example be influenced by ocean waves.

The simulation show that the turbulence in the top layer can have significant impacts on the trajectory of surface drifters. In a separate analysis it was shown that HF radar data can provide valuable information on turbulence parameters in the surface layer. The bottom friction seems to play a smaller role with the exception of areas with strong bathymetry gradients. In a second step trajectories of substances, which have a daily cycle in the depth location, like different phyto and zooplankton types, were investigated. In this case the bottom friction had a higher importance compared to the pure surface drifter simulations. Finally, transports into the German Bight through the westerly and northerly boundary were investigated. The intertidal volume transports for both boundaries are very different and are shown to be strongly dependent on the bottom friction.

2 Activities performed in the Western Adriatic

2.1 General circulation in the Western Adriatic Sea and Gulf of Manfredonia

As one of the major marginal seas of the Mediterranean Sea, the Adriatic Sea is dominated by the Middle and Southern Adriatic cyclonic gyres and the Eastern Adriatic Current and the Western Adriatic Coastal Current systems, as described in Artegiani et al. 1997. In particular, the whole Western coast from the Po River to the Otranto Strait is responsible of a persistent coastal current, which determines complex circulation patterns (meanders) in the Northern part of the Apulian Region, where the Gulf of Manfredonia is located (in the Southern part of the Gargano Peninsula) (Pinardi et al., 2015; Verri et al., 2017). Due to its marine coastal environmental conditions, the Gulf of Manfredonia has been included in the HF Radar network, promoted in the framework of this project, in order to improve coastal monitoring and provide high quality data for setting up high resolution ocean models. The Adriatic-Ionian Forecasting System (AIFS, http://oceanlab.cmcc.it/aifs/) has been used, in the present study, to assess a novel data assimilation system, based on Ensemble Kalman Filter approach, with the purpose to use HF Radar data for improving the ocean current circulation towards the coastal area, focusing on the Gulf of Manfredonia (Figure **1**). AIFS covers the whole Central Mediterranean and is based on the NEMO ocean general circulation model (Nucleus for European Modelling of the Ocean, Madec et al. 2008). It solves the three-dimensional primitive equations on an Arakawa C-grid, assuming hydrostatic ad Boussinesq approximations. The primitive equations are discretized on a horizontal grid at 1/45° resolution using 121 vertical levels and integrated in time using a time-splitting formulation. AIREG is forced by momentum, water and heat fluxes interactively computed by bulk formulae, using the 6h-0.125° horizontal-resolution operational atmospheric data provided by the European Centre for Medium-Range Weather Forecast (ECMWF) (Tonani et al. 2008, Oddo et al. 2009). The atmospheric pressure effect is included as surface forcing. The evaporation is derived from the latent heat flux, while the precipitation is provided by the Climate Prediction Centre Merged Analysis of Precipitation (CMAP) data. Concerning the runoff contribution, the model considers the estimate of the inflow discharge of 75 rivers that flow into the Adriatic-Ionian basin, collected by using monthly means datasets. The Po runoff contribution, instead, is provided by using daily average observations from ARPA Emilia Romagna observational dataset, because of its importance as freshwater input in the Adriatic basin. AIREG is one-way nested into the Mediterranean Sea using Copernicus Mediterranean Monitoring and Forecasting Centre products (temperature, salinity, sea surface height and currents) at daily basis: lateral open boundary conditions are computed using the Flow Relaxation Scheme (Engerdhal, 1995) for temperature, salinity and velocity and the Flather's radiation condition (Flather, 1976) for the depth-mean transport. Interpolation constraint and correction (Pinardi et al. 2003) on the total velocity, which ensure that the total volume transport across boundaries is preserved after the interpolation procedures. AIFS core model has been used for developing the AIFS-EnKF data assimilation system, described further in Sections 2.2. and 2.3.

2.2 Ensemble Kalman Filter

The Kalman filter (Kalman, 1960) is a widely used algorithm to estimate a variable from a series of obserations over time. The Kalman filter exploits knowledge about the prior state of the system to filter statistical noise from the observations, leading to a posterior state that is generally more accurate than the individual observations. One of the main benefits of the Kalman filter over other forms of data fitting is that the filter is recursive, observations can be added sequentially without requiring additional knowledge of past observations. The only information required is the state of the system and its covariance matrix.

The main difficulty in applying the Kalman filter to numerical models of the ocean or atmosphere, lies in the modelling of said covariance matrix. As these models are discretised in space on grids that contain several millions of points, the numerical description of the state of the system is very large. The covariance of such a state is prohibitively expensive to calculate or even store in the memory of a present-day computer.
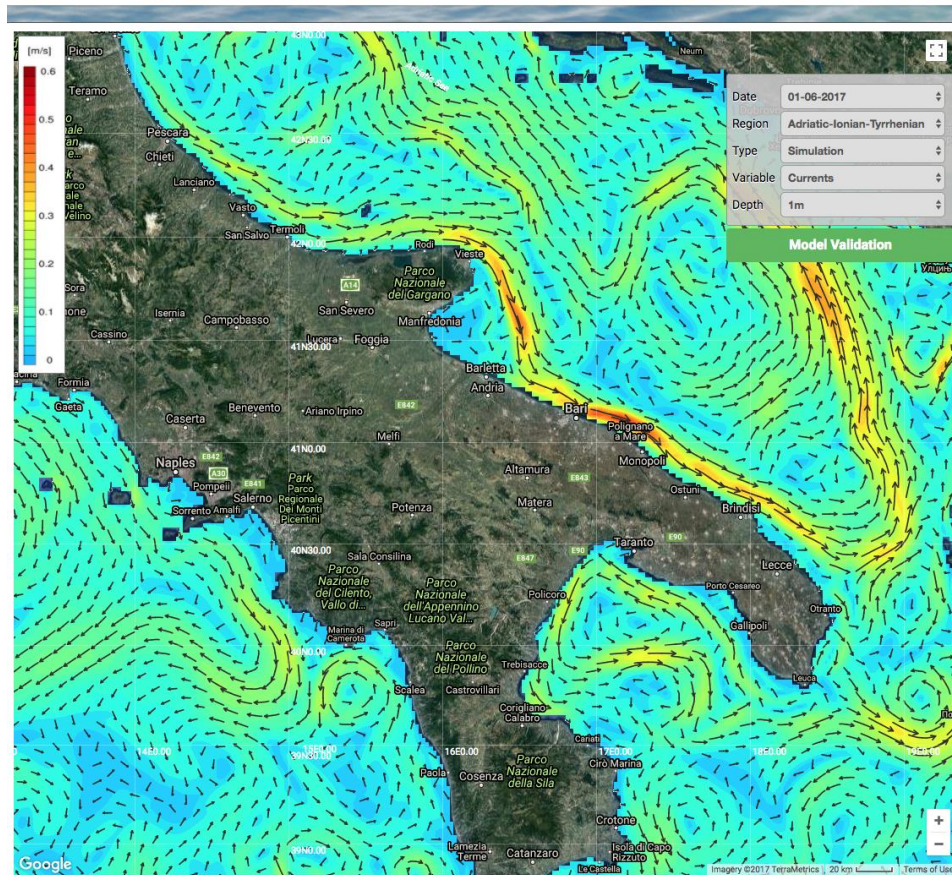
Figure 1: The circulation pattern in the Western Adriatic Sea predicted by AIFS

The Ensemble Kalman Filter (EnKF; Evensen, 1994; Burgers, 1998) is a Monte Carlo approximation to the original Kalman filter. Instead of modelling both the state and covariance of the system, it uses an ensemble of states to model the covariance matrix.

The traditional Kalman filter update equation is given by:

$$\mathbf{x}^a = \mathbf{x}^f + \mathbf{K}\big(\mathbf{y}^o - \mathbf{H}\mathbf{x}^f\big)$$

with $\mathbf{x}^a$ the analysed (posterior) state, $\mathbf{x}^f$ the forecasted (prior) state and $\mathbf{y}^o$ the observation vector. The operator $\mathbf{H}$ is the observation operator, which predicts the value of the observation given the forecasted state of the system. The Kalman gain matrix $\mathbf{K}$ provides the relative weights between the new observation and the existing state, resulting in an update of $\mathbf{x}^f$ to become $\mathbf{x}^a$. The Kalman gain is related to the state and observation covariances as:

$$\mathbf{K} = \mathbf{P}\mathbf{H}^{\mathrm{T}}\big(\mathbf{H}\mathbf{P}\mathbf{H}^{\mathrm{T}} + \mathbf{R}\big)^{-1}$$

with $\mathbf{P}$ the state covariance and $\mathbf{R}$ the covariance of the observations. Here it is important to note that the state vector covariance $\mathbf{P}$ only appears in combination with the observation operator $\mathbf{H}$. Therefore it is not necessary

to calculate the prohibitively large ensemble covariance $\mathrm{cov}(\mathbf{x}^f, \mathbf{x}^f)$ directly, it suffices to calculate the covariance of the state vector with the predicted observations $\mathrm{cov}(\mathbf{x}^f, \mathbf{H}\mathbf{x}^f)$. While the former is of size N_{state}^2, the latter is only $N_{\mathrm{state}} \times N_{\mathrm{observations}}$.

Several variations of the EnKF exist, among them the Ensemble Adjustment Kalman Filter (EAKF; Anderson, 2001) and the Ensemble Sqaure-Root Filter (EnSRF; Whitaker and Hamill, 2002). While the original EnKF needs perturbed observations in order to not underestimate the variance of the ensemble, the EAKF and EnSRF assimilate unperturbed observations. In the EnSRF this is accomplished by multiplying the posterior spread of the ensemble by a factor:

$$\alpha = \left(1 + \sqrt{\frac{\mathbf{R}}{\mathbf{H}\mathbf{P}\mathbf{H}^{\mathrm{T}} + \mathbf{R}}}\right)^{-1}$$

modifying the Kalman filter update equation to:

$$\bar{\mathbf{x}}^a = \bar{\mathbf{x}}^f + \mathbf{K}\left(\mathbf{y}^o - \mathbf{H}\bar{\mathbf{x}}^f\right)$$

$$\mathbf{x}'^a = \mathbf{x}'^f + \alpha\mathbf{K}\left(\mathbf{y}^o - \mathbf{H}\mathbf{x}'^f\right)$$

with bars denoting the ensemble mean and primes denoting the deviation from th mean so that $\mathbf{x} = \bar{\mathbf{x}} + \mathbf{x}'$.

For all practical applications of the Kalman filter in oceanography, the observations are assumed to be uncorrelated, i.e. $\mathbf{R}$ is diagonal. In this case the properties of the Kalman filter allow the observations to be assimilated sequentially, reducing the complexity of the equations considerably. For single observations both $\mathbf{R}$ and $\mathbf{H}\mathbf{P}\mathbf{H}^{\mathrm{T}}$ are scalar values and the calculation of the Kalman gain is trivial.

2.3   The AIFS-EnKF data assimilation system

The ensemble data assimilation system AIFS uses the EnSRF filter to assimilate measurements of temperature, salinity and the surface current velocity measured using HF radar antennas.

Each type of observation requires the implementation of an observation operator $\mathbf{H}$. For temperature and salinity, which are observed quantities as well as state variables of the model, the observation operator simply selects the value closest to the location of the observation. This observation operator does not require additional knowledge of the observation itself and is the same for all observations.

For the HF radar surface velocity the situation is different. The velocities contained in the model state are the zonal (u) and meridional (v) components of the velocity. However, the velocity measured by the radar antenna is the so-called radial velocity, the component in the direction towards or away from the antenna. The observation contains no information on the velocity component perpendicular to this direction. The observation operator needs to project the u and v components of the velocity nearest to the observation onto the axis of the measurement θ:

$$\Omega(u, v, \theta) = -u \sin \theta - v \cos \theta$$

The direction of this axis θ depends on the location of the observation and the location of the antenna, therefore this observation operator is different for each observation.

The EnSRF filter is coupled to the AIFS model in offline mode, i.e. the data assimilation is performed by modifying model restart files rather than by a direct integration of the model and the filter code. Such an online

coupling would require all ensemble members to advance their model in parallel, which requires more computational resources to be available simultaneously and is therefore less practical.

The Kalman filter is performed using a custom implementation of the EnSRF filter in the Python programming language, accelerated using the *numpy* numerical library and parallelized using the *mpi4py* bindings to the *OpenMPI* library.

2.4   Observations and experimental results

HF radar surface current velocity observations are provided by four antennas near the Gulf of Manfredonia, as shown in Figure **2**. Two antennas inside the gulf (Manfredonia and Mattinata), while two others (Pugnochiuso and Vieste) are located on the cape. While the first two antennas provide a good stereo-angle and are therefore able to reconstruct both zonal and meridional components of the surface currents, the two antennas on the cape measure mostly the zonal component.
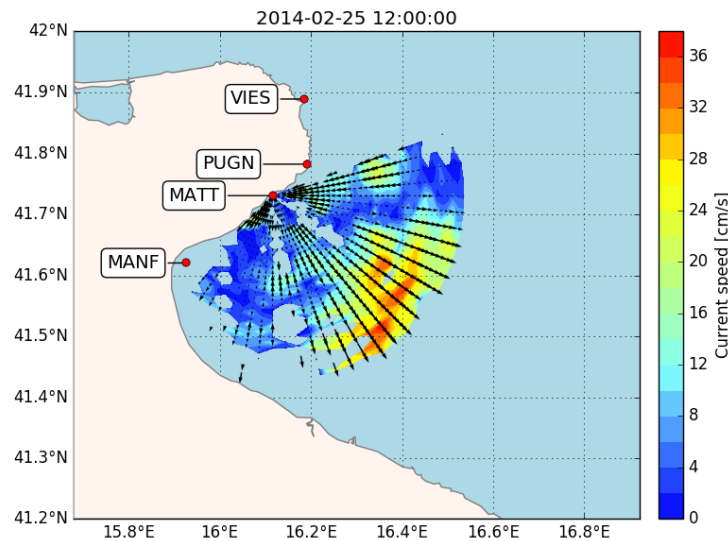

Figure 2: Location of the four HF radar antennas near the Gulf of Manfredonia. The typical range of an antenna is illustrated by superimposing the data measured by the antenna in Mattinata.

The ensemble for the EnSRF is generated from a 12-year historical run (2003-2014). Using the restart files of the nominal model, perturbations are added by sampling the daily average fields for 3 days from each year. These days are spaced 14 days apart and centred on the nominal date. The mean over all days is subtracted from the fields and replaced by the fields of the nominal model. Each day then becomes the perturbation for one ensemble member. The perturbed fields are temperature, salinity and the zonal and meridional velocities.

While the experiment focuses solely on assimilating surface current velocities, the state vector used in the assimilation includes also the temperature and salinity fields. Furthermore the included state extends to a depth of 100m.

Figure **3** shows the change in zonal and meridional surface current velocity (posterior value minus prior value).
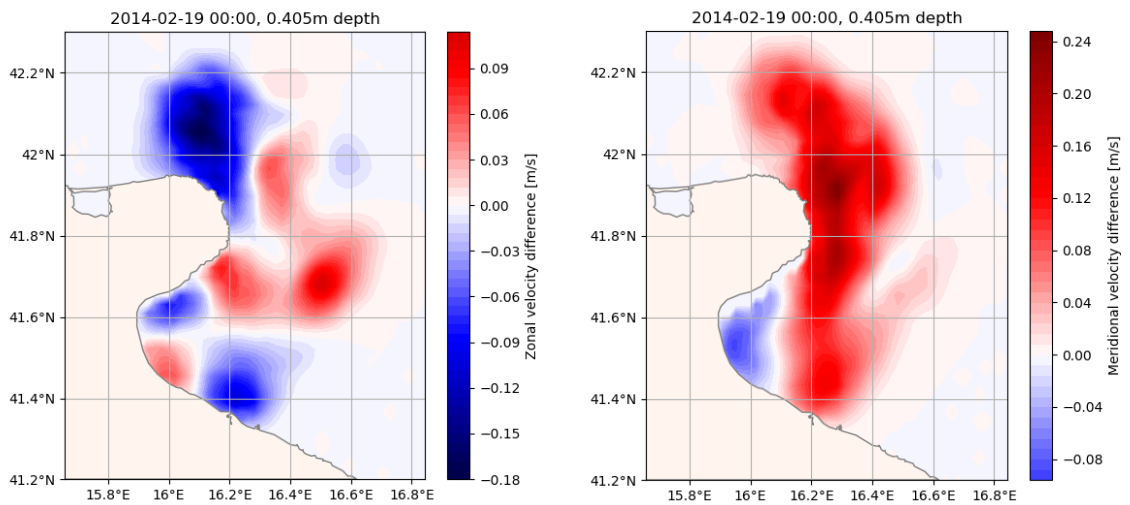
Figure 3: Change in the zonal (left) and meridional (right) surface velocity fields after one assimilation cycle of HF radar surface current velocities.

As the ensemble covariance is calculated for the entire state vector, the assimilation of velocities naturally causes updates to the temperature and salinity fields. This is illustrated in Figure **4**.
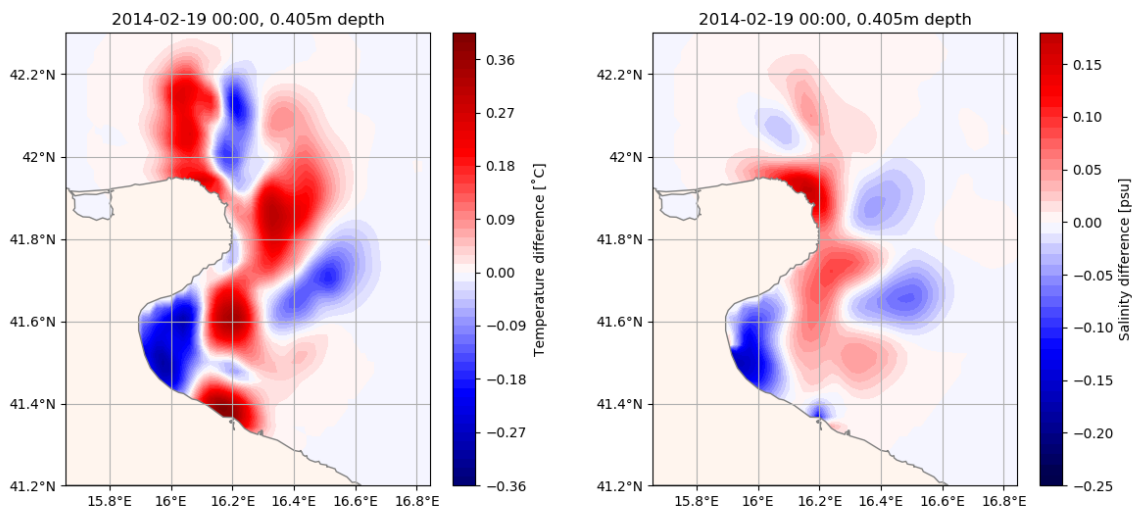

Figure 4: State vector updates for the surface temperature (left) and surface salinity (right) fields as a result of assimilating the radial velocities.

3 Activities performed in the German Bight

3.1 Discription of the general circulation dynamics in the German Bight

The German Bight is characterised by very shallow water with maximum water depth of about 50 m and the dominance of the diurnal tidal component M2. The circulation dynamics is strongly affected by bottom friction, which leads to the generation of higher harmonics in the tidal spectrum. The tidal range is about 3 m and typical current speeds range from 0.5 m/s to 1 m/s. The situation is further complicated by small scale structures in the bathymetry, which often evolve over time due to sediment transport processes. Some areas are so shallow that they fall dry during low tide (Wadden Sea). Usually the water columns is quite well mixed due to the relatively strong tides. Stratification can occur however in the estuaries of the rivers Elbe, Weser and Ems. Typical salinities are between 32 PSU and 5 PSU in the mouth of the river Elbe depending on season.
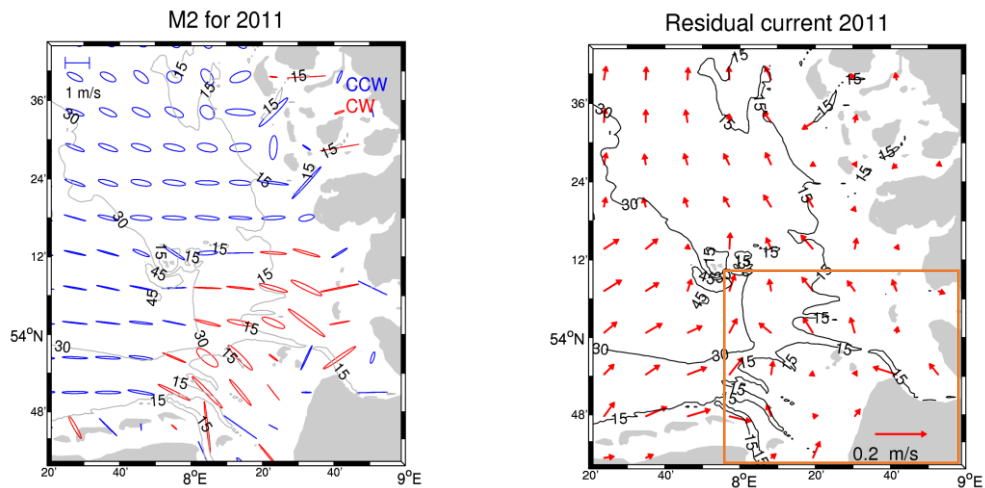

Figure 5: (left) M2 tidal ellipses of surface currents computed with a 3D circulation model. Blue indicates counter-clockwise rotation and red clockwise rotation. (right) Residual surface currents in the German Bight derived from a numerical model. Volume fluxes into the box superimposed in orange are considered in subsequent sections.

Figure 5 (left) shows tidal ellipses of surface currents with blue indicating counter-clockwise sense of rotation and red clockwise sense of rotation. One can see that there are different regimes with very flat ellipses in the southwesterly part and more circular shapes in the north. One can also see that the currents are strongly steered by bathymetry features, in particular in the estuaries of the Weser and Elbe rivers. Figure 6 (right) shows the residual currents obtained by averaging out the tidal component. These currents to a large extend reflect the wind climatology, which is characterised dominant westerly wind directions.

From the numerical modelling point of view the circulation in the German Bight is quite challenging and there are a number of well known systematic and stochastic error sources affecting numerical simulations of the German Bight circulation, such as

- Uncertainties in bottom roughness
- Uncertainties in bathymetry
- Uncertainties about turbulence parameterisation
- Errors in open boundary forcing

- Errors in meteo forcing
- Errors in turbulent kinetic energy

The errors associated with meteo forcing and open boundary forcing usually have a quite short time scale and are therefore a challenge for data assimilation systems, because the information retrieved from observations tend to have only short impacts.

The turbulence parameterisation is of particular relevance for the friction between the top layer measured by the HF radar and the underlying water body, which is dominating the water transports and hence the water levels measured by tide gauges.

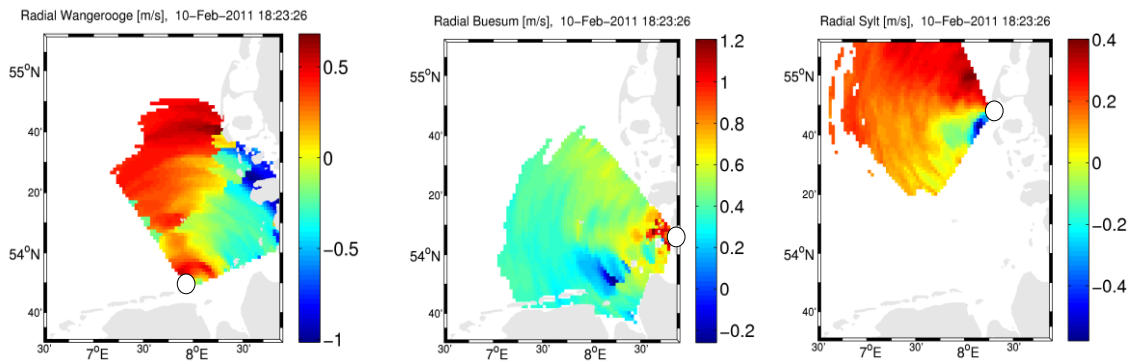## 3.2   Description of the available observation data in the German

Figure 6: Location of the three HF radar antenna stations in the German Bight. The color maps represent exemplary snapshots of measured radial current components.

As part of the COSYNA system three HF radar stations are operated in the German Bight. The locations and typical coverages of the WERA systems are shown in Figure 6. The Büsum and Sylt station use a radio frequency of 10.8-MHz and the Wangerooge station runs at 12.1-MHz. The spatial resolution is 1.5 km in range and 3 deg in azimuth. Because of the relatively high salinities, the German Bight offers good conditions for HF radar operation and the ranges can be up to 120 km depending on specific conditions.

Within COSYNA, the WERA HF radar is run continuously for 58 min. During this time, the stream of radar echoes from all receive antennas of the linear array is sampled at 0.26-s intervals and stored every 128 samples. This leads to about 33-s lasting coherent fractions, which can later be combined to form longer time series as required for further processing. The remaining 2 min within an hour are used to scan the frequency range the HF radar is licensed to be operated at and to select the cleanest frequency range with the lowest RFI possible for the next 58-min radar run The integration time for surface current measurements is 9 min. For ocean current processing, time series of 2048 samples are combined and processed in 20-min steps. These time series are then split up into 13 sliding fractions of 512 samples with 75% overlap. The spectra of these fractions are calculated after dynamic recalibration of the antenna gains by normalizing the first-order Bragg power received by each antenna and applying a Blackman–Harris window. By combining the complex spectra from all antennas of the linear array, beam forming is done in the frequency domain.

Error statistics for the current velocities is derived from the width of the first-order Bragg peak(s). The spectral-averaged radial current velocity u_r and its accuracy Acc are calculated from the Doppler shift of the spectral lines within an interval of i=+/- 8 lines around the Bragg peak locations and their signal to noise ratios.

The surface current measurements generated every 20 minutes are transferred to HZG and are typically available about 30 min after the data were taken.

In addition to the HF radar data tide gauge measurements taken near the island of Helgoland in the centre of the German as well as ADCP data acquired near the FINO-1 research platform were used. Both systems provide measurements every 10 minutes. The FINO-1 ADCP is a bottom mounted device with some well known issues concerning current measurement near the sea surface. For this reason, only measurements 6 m below the surface were taken into account.

3.3   Discription of the DA systems optimised for transport estimations

The data assimilation experiments for the German Bight within WP3.7 were done using a 4DVAR approach based on a 3D barotropic circulation model. The model solves the momentum equations for the zonal and meridional current components u,v

$$\frac{\partial u}{\partial t} = u\,\frac{\partial u}{\partial x} + v\,\frac{\partial u}{\partial y} + g\frac{\partial \eta}{\partial x} - f\,v - \frac{\partial}{\partial z}\left(A\frac{\partial u}{\partial z}\right)$$
$$\frac{\partial v}{\partial t} = u\,\frac{\partial v}{\partial x} + v\,\frac{\partial v}{\partial y} + g\frac{\partial \eta}{\partial y} + f\,u - \frac{\partial}{\partial z}\left(A\frac{\partial v}{\partial z}\right)$$

As well as the continuity equation

$$\frac{\partial \eta}{\partial t} = \frac{\partial U}{\partial x} + \frac{\partial V}{\partial x}$$

which ensures conservation of mass. For the vertical momentum diffusion A a Kochergin type model is used, i.e.

$$A(z) = \alpha\sqrt{(\frac{\partial u}{\partial z})^2 + (\frac{\partial v}{\partial z})^2 + S(z)}$$

In the original version the term S(z) describes the stability of the water column, e.g., the damping of turbulence due to stratified water. In the present barotropic model this term is used as a tuning variable.

As most assimilation approaches, 4DVAR is based on the minimisation of a cost function, which is in our case of the form
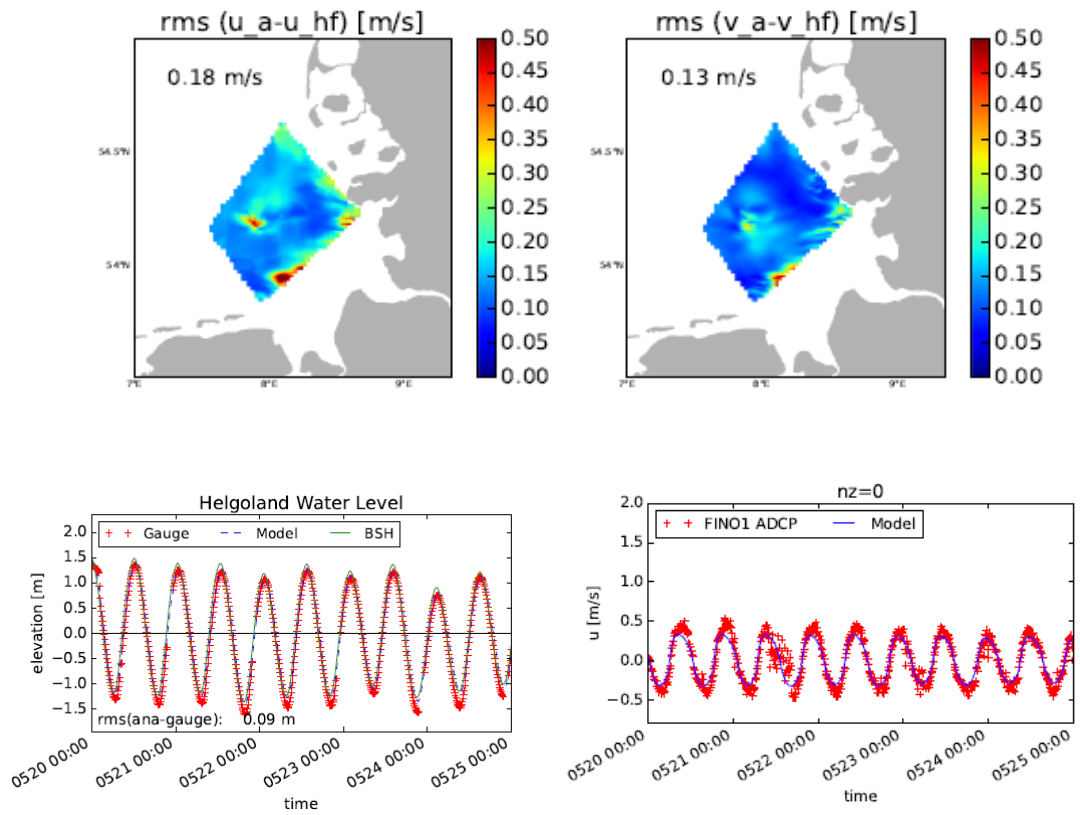
Figure 7: comparison of the analysed model with observations. On the top left and right the rms differences with respect to the HF radar are shown for the zonal (left) and meridional current components. The lower left plot shows the water levels from the analysed model (dashed blue), the Helgoland tide gauge (red crosses) and the model run at the Hydrographic Center. FINO-1 ADCP current measurement in the bottom layer compared to the analysis are presented on the lower right.

$$J(\xi) = 0.5 \sum (y(t_i) - Hx_\xi(t_i))^2 + \cdots$$

with a control vector ξ, an observation vector y, and an observation operator H, which translates the ocean state vectors into observation space. In addition the cost function includes some regularisation terms, which are here omitted for brevity.

The main problem in the minimisation of the cost function is the efficient estimation of the gradient of J with respect to the control vector. In 4DVAR the common approach is to use an adjoint model, which makes use of the fact that numerical ocean models are of the form

$$x(t_i) = M_q M_{q-1} \dots M_2 M_1 x_0$$

Where x_0 is the initial state and the nonlinear operators M evolve this state forward in time. It then turns out that the gradient can be computed as

$$\frac{\partial J}{\partial \xi} = \widehat{M}_1 \dots \widehat{M}_q (y - Hx(t_i)) + \dots.$$

Here, $\widehat{M}_q$ are the linearised transposed model operators and only one term of the sum of the cost function is shown for brevity. This means that the original model has to rewritten in reverse order, which is a quite tedious programming work. Furthermore, some parts of the forward model trajectory have to be available during the backward run. This is realized using direct access files written during the forward run. Having the gradient available the cost function minimisation is performed using a conjugate gradient method with step size control. This exercise has been performed for the 3D barotropic model introduced above resulting in an adjoint model, which can be used for different assimilation and sensitivity studies.

3.4   Application of the DA system to transport estimations in the German Bight

The inverse model introduced in the previous section was used to reduce systematic errors in the 3D barotropic model. For this reason the following parameters were considered as control variables for the optimisation process:

- The bottom drag coefficient, which relates the near bottom current velocity to bottom stress

- The atmospheric Drag coefficient, which relates the 10 m wind to surface stress

- The background momentum diffusion coefficient, which quantify the internal friction

- The initial model state

The following observations were injected into the adjoint model

- The radial components of the three WERA HF radar stations

- Measurements from the tide gauge Helgoland

- ADCP measurements from the FINO-1 ADCP below 6 m

Tide gauge measurements are injected at 10 min intervals and HF radar data at 20 min intervals. The first inversions were performed based on a 54 hrs analysis window. Fig. 3.3 shows comparisons of the inverted model with the observations. One can see reasonably good agreements for both the zonal (top left) and meridional (top right) current component. For the most part the rms is below 15 cm/s. Only in some areas, which are characterised by more complicated small-scale bathymetry features the deviation is higher. Looking at the comparison with the Helgoland tide gauge (lower left), one can see that the agreement with the inverted model is very good in particular for high tides. The low tides are slightly overestimated by the model. To put these results into perspective data from the operational model run at the German Hydrographic Center are superimposed. Fig. 3.3 (lower right) shows a comparison of the analysis with FINO-1 ADCP data at the near bottom level. Again, the agreement is very good. taking into account that the ADCP data at times are affected by considerable noise.

There is very little a priori information about suitable settings for bottom roughness and internal friction and the values used for the first guess runs were very different from the optimised parameters used in the analysis. In the following the improvements achieved by the inversion are illustrated by comparing the analysis to different first guess runs. In the first set of experiments surface drifter trajectories were simulated by solving the ordinary differential equation

$$\begin{pmatrix} \dot{x}(t) \\ \dot{y}(t) \end{pmatrix} = \begin{pmatrix} u(x(t), y(t), z = H, t) \\ v(x(t), y(t), z = H, t) \end{pmatrix}$$

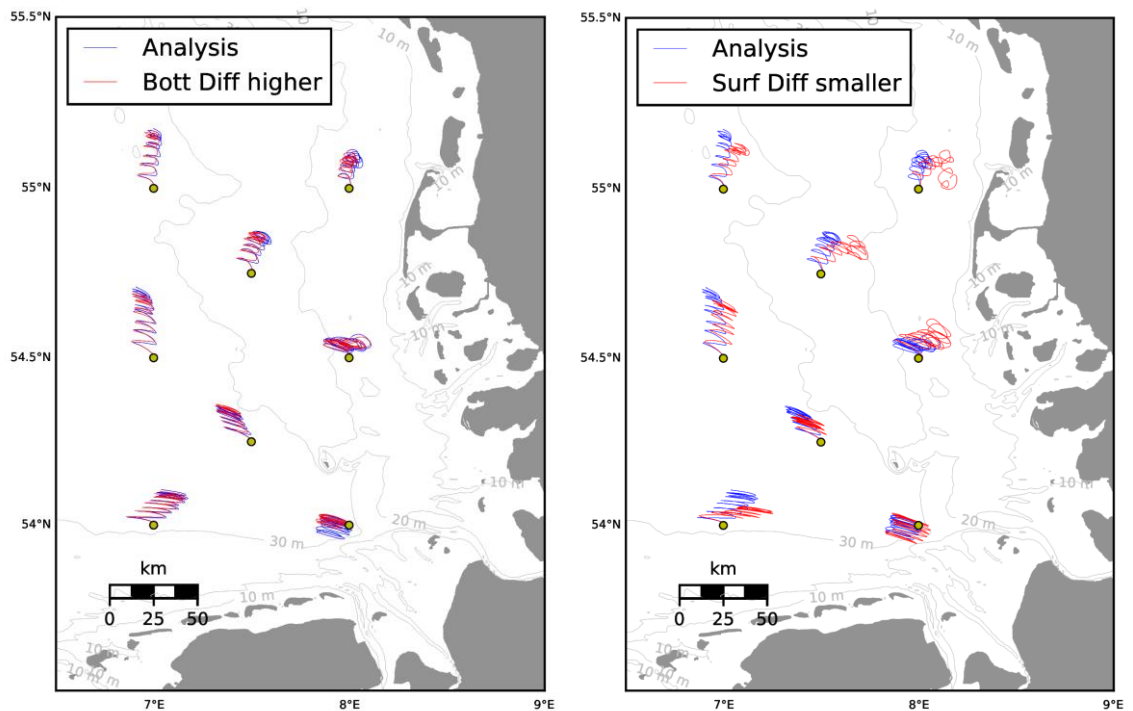This was done using a Euler forward scheme with 5 min time stepping.

Figure 8: Comparisons of surface drift trajectories derived from analysed model runs (blue trajectories) in comparison to first guess runs (red curves) over a period of five days. The yellow dots indicate the release locations. The red trajectories in the left plot are based on a higher estimate for the bottom roughness. The red trajectories on the right are related to a reduction of the momentum diffusion in the surface layer. In addition the 10m, 20m and 30 m isobaths are superimposed as grey lines.

Figure 8 shows simulations over a period of 5 days for 8 simulated drifters released at different locations in the German Bight. The release points are indicated by yellow dots and isobaths for 10 m, 20 m, and 30 m are superimposed as grey lines. In the left plot the surface drifter trajectories derived from the analysis (in red) are compared with a first guess run with 10 times rougher bottom surface (in blue). One can see that the bottom roughness does not seem to have a very strong effect except for the drifter on the lower right, which happens to be released at a location with quite strong bathymetry gradient. The two drifters in the upper right released in water depth below 20 m show a slightly stronger sensitivity with respect to bottom roughness, but the effect is still small. Figure 8 (right) shows again a comparison of the analysis with a first guess run, but this time the first run differs by smaller momentum diffusion in the top layer (10 times smaller). One can see that this has a quite substantial impact on the surface drifter trajectories. The reason for this observations is the role that the momentum diffusion plays for the connection of the top layer to the underlying water mass. If the turbulence in the top layer is small the upper water layer experiences less friction and can be more easily moved around by both pressure gradients and the wind forcing. As can be seen on the map, it is not easy to predict in which areas this mechanism has the strongest impact on the trajectories.
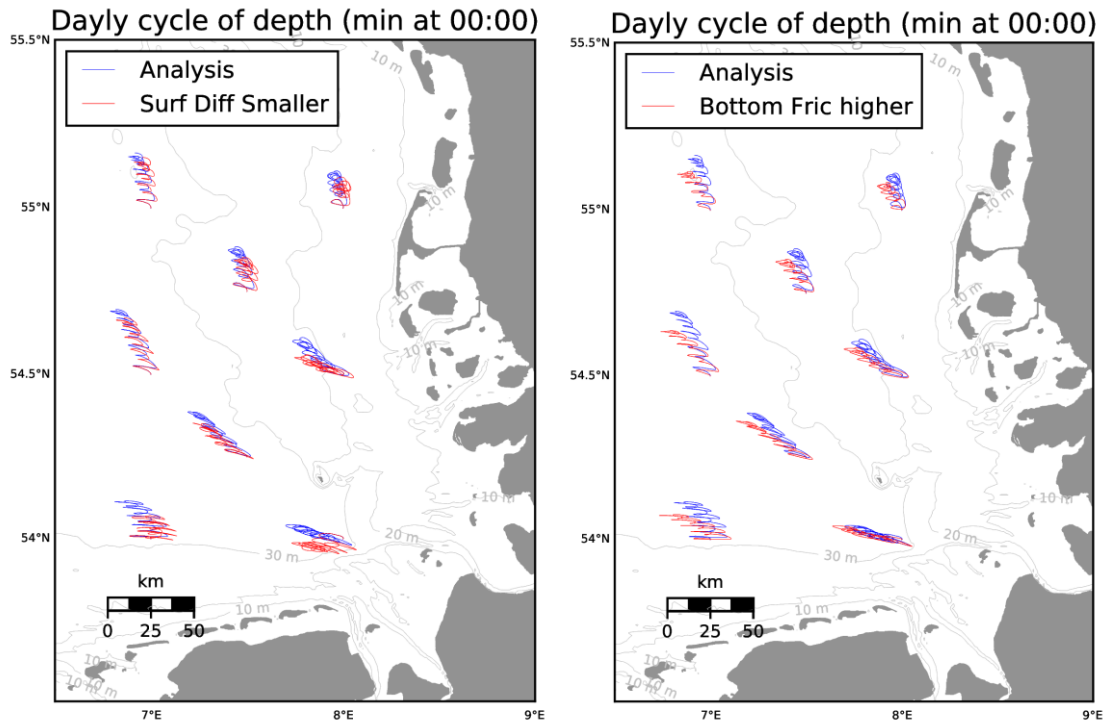
Figure 9: Comparisons of drift trajectories derived from analysed model runs (blue trajectories) in comparison to first guess runs (red curves) over a period of five days. To simulate biological active material a daily cycle of depth position was assumed with the maximum distance to the water surface at midnight. The yellow dots indicate the release locations. The red trajectories in the left plot are based on a higher estimate for the bottom roughness. The red trajectories on the right are related to a reduction of the momentum diffusion in the surface layer. In addition the 10m, 20m and 30 m isobaths are superimposed as grey lines.

In a second set of experiments the advection of substances within the water body was analysed. The background for this study was the fact that biological material (e.g., zooplankton, phytoplankton) often moves up and down in the water column depending on light conditions. Because the current conditions change at lower depth this behaviour has an impact on the respective trajectories. In a first approach we assumed that the vertical position follows a simple daily cycle with a near surface position at noon and the lowest positions at midnight. We are aware that this is a very simplistic view for most zooplankton or phytoplankton types, but the goal here was to illustrate the potential role of the vertical current structure on the advection of biological substances and not to simulate the evolution of biological species in a fully realistic way. Results achieved based on these assumptions are shown in Figure 9. Again trajectories derived from the analysis run (in blue) are compared with first guess runs (in red). The first guess run on the left was characterised by lower surface turbulence and the first guess run on the right had a rougher ocean bottom. The release locations were the same as those used in Figure 8. First of all, comparing these trajectories inside the water body to the surface trajectories shown in Figure 8 one can see that the vertical structure of the current field has a significant impact on the advection of materials. Most of the trajectories at the surface have a slightly more easterly direction, which is likely due to the fact that these simulated drifters are more strongly affected by the near surface wind field. Comparing the analysis with the first guess runs it is evident that the bottom roughness now has a bigger impact than for the pure surface drifter case. This makes sense because the deeper layers, where the material now spends more time, is more affected by the bottom. The role of the surface turbulence illustrated in Figure 9 (left) is reduced compared to the surface advection situation, because the material spends less time at the surface.
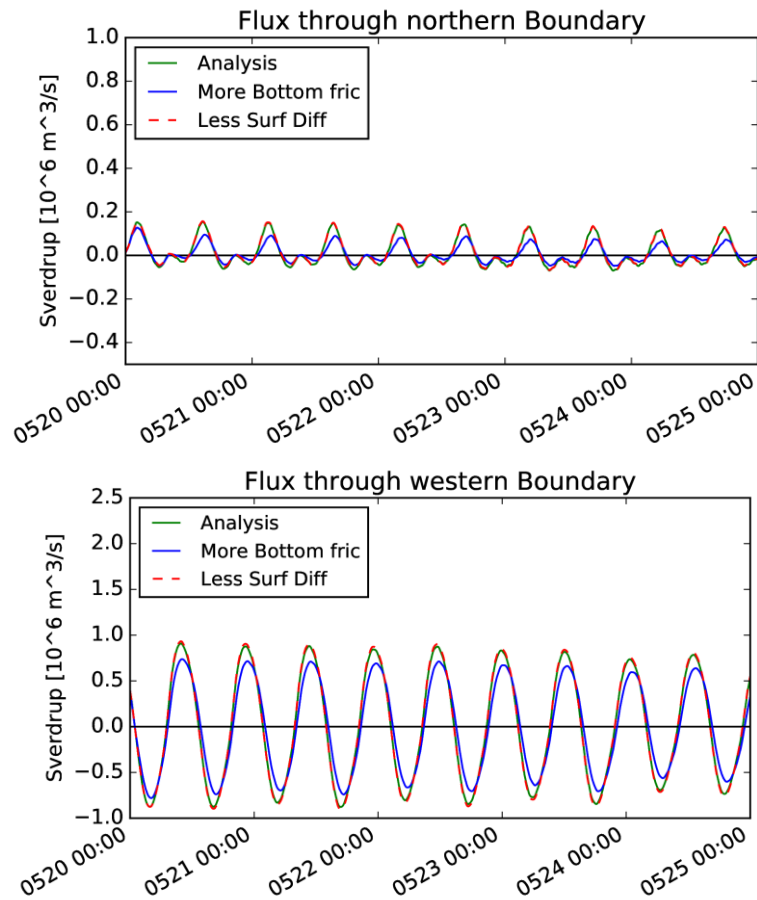
Figure 10: Volume fluxes through the northern boundary and the western boundary of the box depicted in Figure 3.1 (right). The colors refer to analysed run (green) the first run with stronger bottom friction (blue) and the first guess run with reduced momentum diffusion in the surface layer.

The last set of experiments was concerned with volume transports in the German Bight, which are of relevance for biological processes as well. For this purpose a control volume as indicated by the orange box in Figure 5 (right) was considered. This box only has exchange with the surrounding ocean through the westerly and the northerly open boundary. In the flux computations not only the surface currents perpendicular to these boundaries, but also the respective water levels have to be taken into account. Fig. 3.6 shows time series of transports in units of Sverdrup for the westerly boundary (left) and the northerly boundary (right). Again the analysis (green line) was compared to the first guess run with increased bottom friction (blue line) and the first guess run with reduced top layer turbulence (dashed red line). The first thing to notice is that this is an interesting system with substantially more intertidal volume fluxes through the westerly boundary (about +/- 1 Sverdrup) than through the northerly boundary (between -0.05 and 0.15 Sverdrup). Because of volume conservation the residual currents through both boundaries are about the same and of the order of 0.05 Sverdrup. The rivers Elbe and Weser contribute some volume, but this amounts to only about 1000 m^3/s =0.001 Sverdrup, which is one order of magnitude lower than the fluxes through the westerly and northerly boundaries. Looking at the impact of the surface roughness and the turbulence in the top layer it is evident that the bottom friction is a more important factor for volume fluxes.

4 References

J. L. Anderson, "An Ensemble Adjustment Kalman Filter for Data Assimilation", Monthly Weather Review, 129 (2001) 12 2884--2903.

A. Artegiani, Paschini, E., Russo, A., Bregant, D., Raicich, F., Pinardi, N., "The Adriatic Sea general circulation. Part ii: Baroclinic circulation structure", Journal of Physical Oceanography 27 (8), 1515–1532. http://dx.doi.org/10.1175/1520- 0485(1997)027h1515:TASGCPi2.0.CO;2.

G. Burgers, P. J. van Leeuwen, and G. Evensen, "Analysis Scheme in the Ensemble Kalman Filter", Monthly Weather Review, 126 (1998) 6 1719--1724.

G. Evensen, "Sequential data assimilation with a nonlinear quasi-geostrophic model using Monte Carlo methods to forecast error statistics", Journal of Geophysical Research: Oceans, 99 (1994) C5 10143-10162.

R. E. Kalman, "A New Approach to Linear Filtering and Prediction Problems", Journal of Basic Engineering, 82 (1960) 1 35-45.

N. Pinardi et al., "Mediterranean Sea large-scale low-frequency ocean variability and water mass formation rates from 1987 to 2007: A retrospective analysis", Progress in Oceanography, 132 (2015), 318-332.

G. Verri, Pinardi, N., Oddo, P., Ciliberti, S.A., Coppini, G., "River runoff influences on the Central Mediterranean overturning circulation", Climate Dynamics, DOI 10.1007/s00382-017-3715-9

J. S. Whitaker and T. M. Hamill, "Ensemble Data Assimilation without Perturbed Observations", Monthly Weather Review, 130 (2002) 7 1913-1924.